J Mater Sci: Mater Electron (2016) 27:3668–3674
DOI 10.1007/s10854-015-4206-6

CrossMark

Investigations on morphological and electrical studies of sputtered MoO_3 films

V. Nirupama[1,2] · S. Uthanna[2]

Received: 30 June 2015 / Accepted: 8 December 2015 / Published online: 17 December 2015
© Springer Science+Business Media New York 2015

Abstract Molybdenum oxide (MoO_3) films were deposited by sputtering of molybdenum target under different substrate temperatures 303–673 K using DC magnetron sputtering. Sputtered MoO_3 films under optimized conditions show nano structured grains whose size is around 140 nm, while roughness of the films will increase from 5.7 to 70 nm due to grain growth and mechanical stress development on the films. The microhardness of MoO_3 films increased from 0.49 to 1.28 GPa with increase of substrate temperature. The electrical resistivity of the MoO_3 films at 303 K is $0.27 \times 10^4\ \Omega$ cm increases to $1.9 \times 10^4\ \Omega$ cm with increase of substrate temperature and then decreases at higher substrate temperature. The activation energies of the films at higher temperature region was varied from 0.98 to 1.30 eV while at low temperature region the activation energies were in the range 0.02–0.10 eV. The refractive index of MoO_3 films increases from 2.03 to 2.18 with increase of substrate temperature from 303 to 673 K due to packing density. The change in morphological and microhardness properties can be explained due to the existence of a mixed phases and stoichiometric films.

1 Introduction

To meet the required demands of sensing technology, materials must be deposited with suitable compositions, crystallographic structure and morphology, mechanical, electrical and optical properties. Transition metal oxides such as molybdenum oxide (MoO_3), vanadium oxide (V_2O_5) shows different characteristics which can be used in fabrication of nanostructured devices like super capacitors [1], memory devices [2], chemical and biological sensors, spintronics and biomedicine [3–5]. More over molybdenum oxide (MoO_3) shows versatile behaviour like chromism and optical modulation [6–8]. Hence it is desirable to study the properties of the molybdenum oxide at the nanoscale for its effective utilization. Among transition metal oxides, Molybdenum oxide has been widely used for different applications because of its interesting structural, mechanical and electrical properties. However, nanosized MoO_3 films can offer large surface area to volume ratio and good electrochemical stability due to energy difference between a cation d^n and either a d^{n+1} or d^{n-1} configuration is often small and has wide range of oxidation states [9]. Hence they are more sensitive to environment. To study the structural sensitive properties, far off MoO_3 films were deposited under various deposition techniques such as thermal evaporation [10], pulse laser deposition [11], chemical vapour deposition [12, 13], sol–gel process [14], spray pyrolysis [15, 16], electron beam evaporation [17, 18], DC sputtering [19–21] and RF sputtering [22–24]. Among these techniques, DC magnetron sputtering is often industrially practiced method for the growth of oxide films on large area substrates. The physical behaviour of the deposited oxide films by above method depends on the oxygen partial pressure, substrate temperature, sputtering power and substrate bias voltage. In our earlier investigations, MoO_3 films were deposited by DC magnetron sputtering at oxygen partial pressures [25], substrate temperatures [26], sputtering power [27] and substrate bias voltage [28] and studied their structures, electrical and optical properties. The main objective of this paper

✉ V. Nirupama
nirupamav_79@yahoo.com

[1] Sree Vidyanikethan Engineering College, Tirupati 517 502, India

[2] Department of Physics, Sri Venkateswara University, Tirupati 517 502, India

includes the detailed study of microstructural characterization of the films by studying their composition, surface roughness using morphology, mechanical, electrical and optical properties supportive to the previous results. In future, these properties can be utilized to deposit the X-MoO_3 (X = Zn, W) films while measuring sensitivity for NH_3 and H_2S gases.

2 Experimentation

DC reactive magnetron sputtering technique was employed for deposition of molybdenum oxide films on to glass and silicon substrates by sputtering of molybdenum target at fixed oxygen partial pressure of 2×10^{-4} mbar and at different substrate temperatures in the range 303–673 K. The sputter chamber was evacuated to an ultimate pressure of 5×10^{-6} mbar by using diffusion pump backed by rotary pump. Penning and Pirani gauges were used to measure the pressure in the sputter chamber. Circular planar magnetron target assembly of 50 mm diameter with sputter down configuration was employed for deposition of the experimental films. After achieving the ultimate vacuum, required quantities of reactive gas of oxygen and sputter gas of argon were introduced into the sputter chamber through fine controlled needle valves. The flow rate of oxygen and argon were individually controlled by Tylan mass flow controllers. Continuously variable DC power supply of 1000 V and 1 A was used for sputter deposition of the films. The deposited films were characterized for their chemical composition and core level binding energies were determined by X-ray photoelectron spectroscope (KRATOS-AXIS 165). Crystallographic structure and crystallite size of films was determined with X-ray diffractometer (Seifert Model 1003 TT). Surface morphology of the deposited films were analysed by using atomic force microscopy (AFM) Nanoscope III. The mechanical properties like micro hardness developed within the films have been measured using Nano Indenter XP instrument. The electrical resistance of the films was measured Keithley (Model 610 C) electrometer. The optical transmittance of the films was recorded by UV–Vis–NIR (Hitachi U-3400 UV–Vis–NIR) double beam spectrophotometer. The deposition parameters maintained during the preparation of the MoO_3 films are given Table 1.

Table 1 Deposition parameters fixed for the growth of the MoO_3 films

Sputter target	Molybdenum (50 mm diameter)
Target to substrate distance	75 mm
Ultimate pressure (P_u)	5×10^{-6} mbar
Sputter pressure (P_w)	4×10^{-2} mbar
Oxygen partial pressure (pO_2)	2×10^{-4} mbar
Substrate temperature (T_s)	303–673 K
Sputtering current	250 mA

3 Results and discussions

The dependence of the deposition rate of MoO_3 films on the substrate temperature is shown in Fig. 1. The deposition rate of the films increased from 21.45 to 23.62 nm min^{-1} when substrate temperature increased from 303 to 523 K. The initial increase of deposition rate at lower substrate temperature was attributed to the lower adatom mobility on the substrate surface. Further increase of substrate temperature to 673 K, the deposition rate start to decreased and reached to a minimum value of 22.56 nm min^{-1}. The decrease of deposition rate at higher substrate temperatures may be due to the balance between the number of atoms arriving on the substrate and atoms leaving from the substrate surface which resulted re-evaporation of the films hence of lower deposition rate [29].

Figure 2 shows X-ray diffraction profiles of MoO_3 films deposited at different substrate temperatures. The film deposited at room temperature (303 K) is dark in colour which shows no diffraction peaks can be attributed to low deposition rate. Absence of diffraction peaks at lower temperature would indicate the presence of different molybdenum species [30]. As the substrate temperature increased to 423 K, weak intense peaks at $2\theta = 12.8^{o}$, 23.04°, 25.70°, 39.05° and 49.29° were observed. They were related to the (020), (011), (040), (060) and (002) reflections indicate the onset of crystallization. As substrate

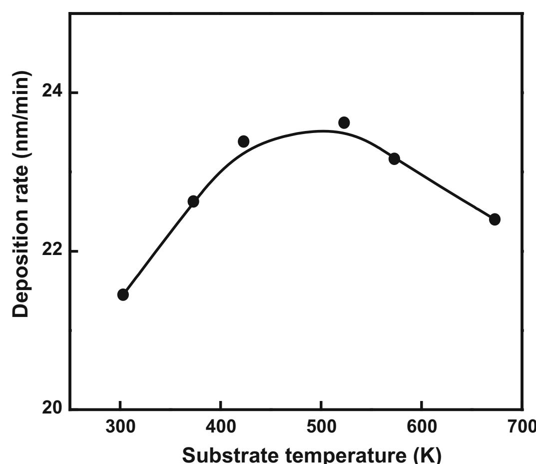

Fig. 1 Dependence of deposition rate of MoO_3 films with different substrate temperatures

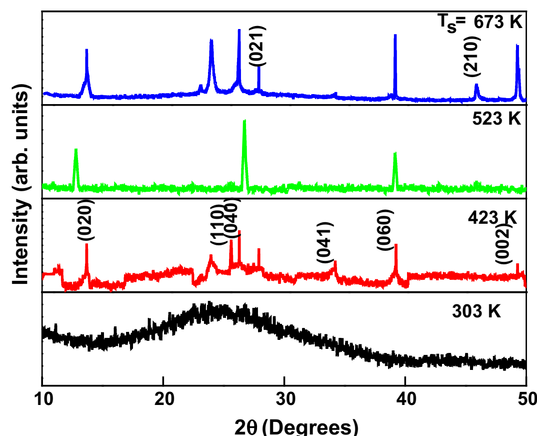

Fig. 2 X-ray diffraction profiles of MoO_3 films deposited at different substrate temperatures

temperature increases to 523 K, relative intensities of the (020), (040) and 060) peaks increased with disappearance of (011) reflection. Further increase of substrate temperature from 523 to 673 K, phase transition took place from α-phase to β-phase (orthorhombic and monoclinic). This result is confirmed from FWHM of the most intense peak (040) reduces as substrate temperature increases from 523 to 673 K and such variation was also observed by Martinez et al. [15]. The crystallite size of the films was evaluated from the diffraction peak of (040) using Scherrer's relation [31].

$$L = \frac{0.9\lambda}{\beta \cos \theta} \quad (1)$$

where β is the full width at half maximum (FWHM) intensity. The FWHM and crystallite size of the films for the peaks (040) increases from 25.6 to 140 nm with increase of temperature from 303 to 523 K, and then decreases to 82 nm as the temperature increased to 673 K. Intensity of the peak (040) increased gradually with increase of substrate temperature from 303 to 523 K due to enhancement in the horizontal velocity of the adatoms and condensation coefficient during cluster formation which causes an improvement in crystallinity [32]. The films deposited at 673 K showed a phase change from α-phase to α- and β-phases with a predominant (021) and (002) peaks, which might be due to the structural reorientation (or) re-evaporation of molybdenum results in the decrease of crystallite size. Dhanasankar et al. [14] observed that the grain size of sol–gel processed MoO_3 films decreased from 30 to 29 nm with increase of annealing temperature from 473 to 523 K respectively. Figure 3 shows the XPS spectrum of the MoO_3 film deposited at 523 K. The peak observed at 530.54 eV related to the core level binding energy of oxygen O 1s and the peaks located at 415.7 and 395.55 eV were the molybdenum Mo $3P_{1/2}$ and Mo $3P_{3/2}$ respectively. The peak situated at 282.3 eV related to the carbon C 1s due to the contamination on the surface of the films because of exposure to the atmosphere. The C 1s peak was disappeared when the films were sputter etched by argon ion bombardment for 5 min in the XPS system. The peaks observed around 232.77 and 235.90 eV were of Mo $3d_{5/2}$ and Mo $3d_{3/2}$. The peaks seen at about 66 and 40.42 eV were the core levels of Mo 4s and Mo 4p respectively. The spectrum of the Mo 3d doublet at 523 K and oxygen (O 1s) core levels binding energy of MoO_3 films formed at different substrate temperatures is shown in Fig. 4. Table 2 shows the core level binding energies of the molybdenum and oxygen present in the MoO_3 films. The core level binding energies of Mo $3d_{5/2}$ and Mo $3d_{3/2}$ peaks increased from 232.44 to 232.89 and 235.58 to 236.01 eV with the increase of substrate temperature from 303 to 623 K, which was discussed in detail [23]. The core level binding energy of oxygen in deposited films was increased from 530.29 to 530.68 eV with the increase of substrate temperature from 303 to 673 K respectively. The increase in the binding energy of O 1s with the increase of substrate temperature was attributed to the deficiency of oxygen ion vacancies. It is revealed that the MoO_3 films formed at a higher substrate temperature (>523 K) were polycrystalline due to deficiency in oxygen ion vacancies which confirms from XRD data.

Surface morphology plays an important role on sensitivity of the films and significantly varies with substrate temperature. The AFM micrographs of the films are shown in Fig. 5. MoO_3 films deposited at 303 K showed small islands which were homogenous and uniform. The size of initially formed nuclei would be small due to the substoichiometric nature as revealed by XPS and XRD. As the substrate temperature increased from 423 to 673 K, the size of the nuclei also increases and grown like sharp needle structure. When substrate temperature increased to 673 K,

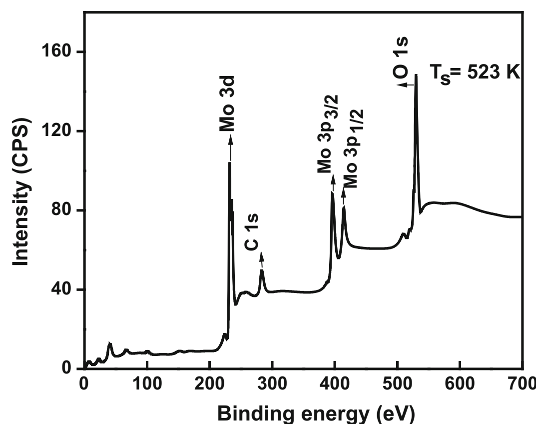

Fig. 3 XPS spectrum of MoO_3 films deposited at substrate temperature of 532 K

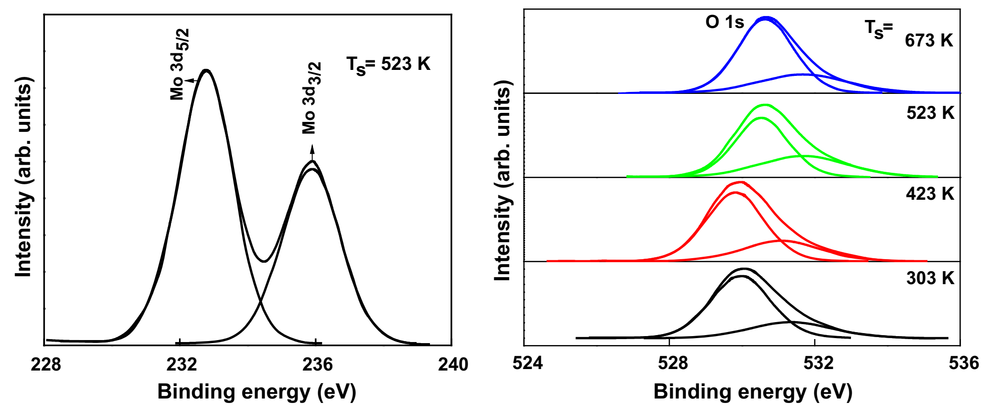

Fig. 4 XPS core level binding energies of Mo 3d and O 1s of MoO_3 films formed at different substrate temperatures

Table 2 Core level binding energies of molybdenum and oxygen in the MoO_3 films formed at different substrate temperatures

Substrate temperature (K)	Binding energy (eV)				
	Mo $3d_{5/2}$		Mo $3d_{3/2}$		O 1s
	Mo^{6+}	Mo^{5+}	Mo^{6+}	Mo^{5+}	
303	232.44	231.23	235.58	234.21	530.29
423	232.49	–	235.64	–	530.17
523	232.77	–	235.90	–	530.54
673	232.89	–	236.01	–	530.68

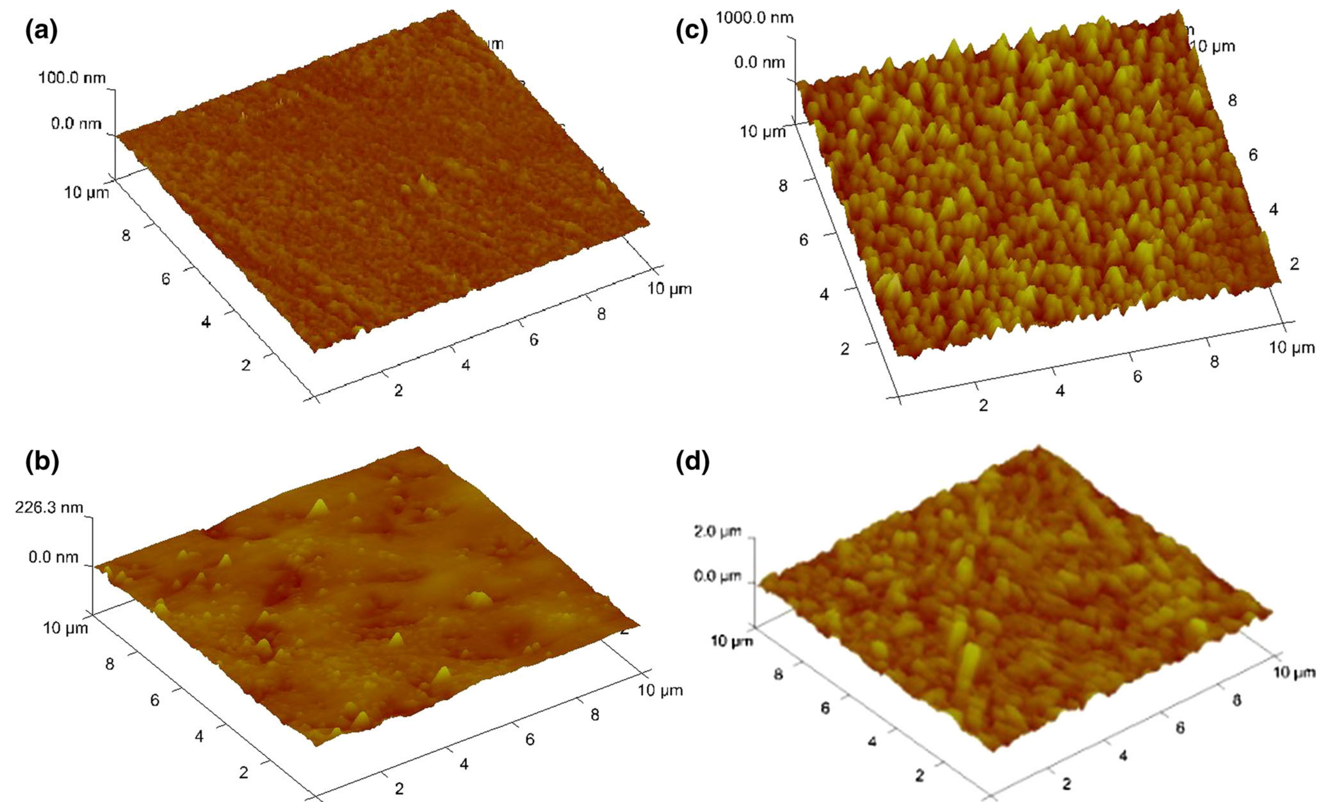

Fig. 5 AFM micrographs of MoO_3 films formed at different substrate temperatures. **a** 303 K, **b** 423 K, **c** 523 K, **d** 673 K

grains appear to be quasi cylindrical nuclei in random direction; this is due to the polycrystalline nature as confirms from XRD studies. Such a morphological nature of MoO_3 films was reported by thermal and electron beam evaporated films [33, 34]. AFM also used to measure the root mean square roughness (R_{rms}) of the films [35]. Figure 6 shows the variation of surface roughness (R_{rms}) and peak-to-valley roughness (R_{p-v}) with substrate temperature. From the Fig. 6 it is observed that both R_{rms} and R_{p-v} values increased with increase of substrate temperature and roughness of the films were in the range 5.70–71.4 nm. Although both R_{rms} and R_{p-v} values are seems to be different, each value can describe more specific morphology. From AFM it has been observed that the grain size of the films increased from 50 to 226 nm due to segregation of crystallites. Mohamed et al. [36] showed the roughness of as deposited films increased with the increase of annealing temperature which attributes the grain growth and the stress builds up in during heating and subsequent cooling. Core et al. [37] noticed the R_{rms} and R_{max} of the annealed MoO_3 film were 144 and 795 nm. It clearly indicated that surface roughness of the films increases due to grain growth and mechanical stress development within the films.

Figure 7 shows the microhardness of MoO_3 films deposited at different substrate temperatures. Microhardness of MoO_3 films increased from 0.49 to 1.28 GPa with increase of substrate temperature from 303 to 673 K. Low value of microhardness of the films deposited at 303 K was due to amorphous nature and the presence of oxygen ion vacancies [38]. The microhardness of stoichiometric MoO_3 films deposited at 523 K was 1.12 GPa due to improvement in the packing density by partial filling oxygen ion vacancies. Further increase of substrate temperature to 673 K, microhardness increases to 1.28 GPa due to enhanced surface roughness of the polycrystalline MoO_3

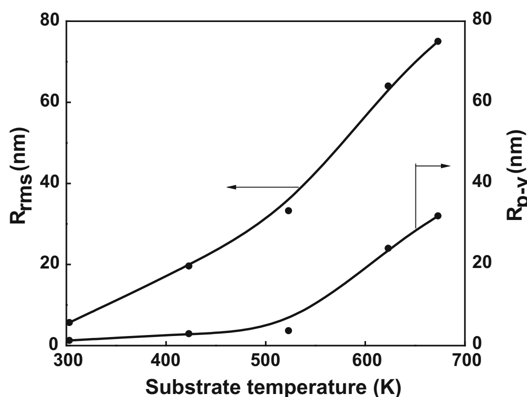

Fig. 6 Variation of surface roughness (R_{rms} and R_{p-v}) values of MoO_3 films with substrate temperature. **a** 303 K. **b** 423 K. **c** 523 K. **d** 673 K

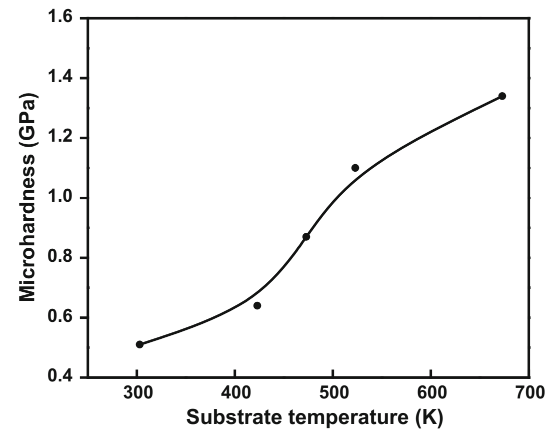

Fig. 7 Variation of microhardness of MoO_3 films with substrate temperature

[30]. Figure 8 shows the dependence of stress on the substrate temperature of MoO_3 films. The internal stress in the films was calculated using the relation,

$$\sigma_{\text{intrinsic}} = Y(a - a_0)2\gamma a_0 \quad (2)$$

Here a is the lattice constant, a_0 the bulk lattice constant and γ the Poisson's ratio. From Fig. 8 it is seen that internal stress of the films deposited at room temperature was −430 GPa indicates the compressive stress. As substrate temperature increased to 373 K, compressive stress decreases to −160 GPa. Further increase of substrate temperature from 523 to 673 K the stress had transformed from compressive to tensile and reached to a value 36 GPa. The compressive stress developed within the film was up to 423 K attributed to lattice distortions because of amorphous nature of the films and presence of mixed oxidation state of MoO_3 which is revealed by XRD. The tensile stress which starts to build up above 523 K is clear evidence for improvement in the grain size as seen in AFM. Figure 9

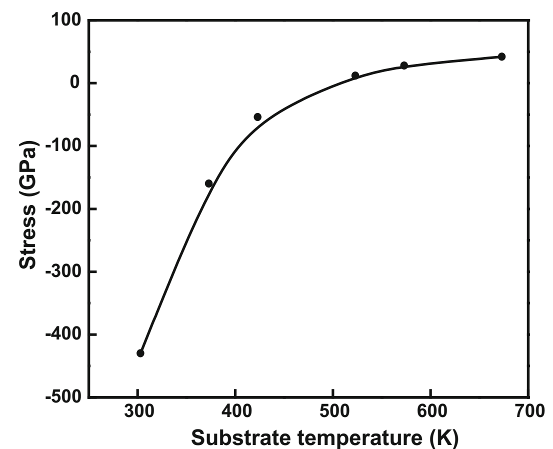

Fig. 8 Variation of stress developed in the molybdenum oxide films with substrate temperature

shows the variation of electrical resistivity of MoO_3 films with substrate temperature. The electrical resistivity of MoO_3 films formed at 303 K was low value of 2.7×10^3 Ω cm due to both valence band and conduction band is free from charge carriers. As substrate temperature increases to 423 K, the electrical resistivity increases to 1.9×10^4 Ω cm due to donor atoms get ionized and increase in the electron concentration in the conduction band. Hence resistivity increases due to electron mobility and also due to presence of substitution ions during deposition [39]. As temperature increases to 523 K, resistivity decreases to 3.5×10^4 Ω cm due to increase in thermal energy leading to the formation of compact crystalline MoO_3 films with cylindrical structure grains size and due to electron charge transfer. Though the carrier mobility decreases with increase of substrate temperature to 673 K, its effect is overcome by the large number of carriers produced by thermal agitation, resulting in reduction in grain size. Hady et al. [40] also observed that resistivity of sputtered MoO_3 films decreases at higher substrate temperatures; this is due to increase in grain size. Figure 10 shows the dependence of log σ with the (1000/T) for the films formed at different substrate temperatures. From the Fig. 10 it is clear that the electrical conductivity of the films increased exponentially with the increase of temperature. The curve supports two transport mechanisms with in deposited films. The activation energies of the films deposited at higher temperature region was varied from 0.98 to 1.30 eV while at low temperature region the activation energies were in the range 0.02–0.10 eV. These activation energy values indicate that the electrical conduction in the films deposited at high temperatures was due to the band to band transition at low temperatures due to hopping conductivity [41]. It is attributable to the formation of the large number of oxygen ion vacancies in the

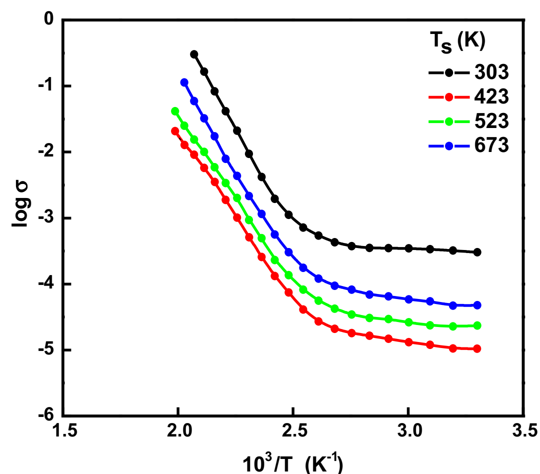

Fig. 10 Plot of log σ versus 10^3/T of MoO_3 films formed at different substrate temperature

deposited films. It is to mention that Krishna Kumar [42] achieved the activation energies of 1.35 and 0.46 eV at high and low temperature region in thermal evaporated films, while low activation energy of 0.68 and 0.78 eV at higher temperature region in electron beam evaporated films [17]. Martinez et al. [15] also reported that activation energy was 0.9 eV at high temperatures where as 0.02 eV at low temperatures. It was reported that the optical band gap increased from 3.03 to 3.22 eV with increase of substrate temperature from 303 to 523 K. And it decreased to 3.15 eV with further increase of substrate temperature to 623 K [26]. The variation of refractive index with the substrate temperature at particular wavelength of 500 nm is shown in Fig. 11. The refractive index of MoO_3 films deposited at room temperature was 2.03. As the substrate temperature increased to 673 K, the refractive index of the films increases to 2.18. Low refractive index in the films

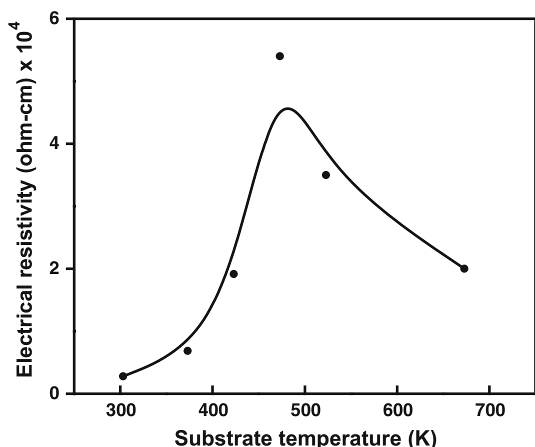

Fig. 9 Variation of electrical resistivity of MoO_3 films with substrate temperature

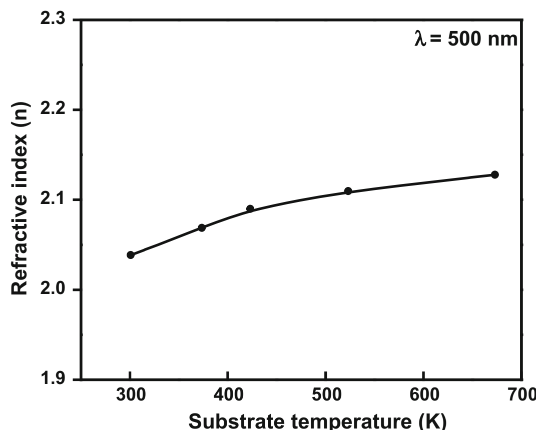

Fig. 11 Variation of refractive index of MoO_3 films with substrate temperatures at λ = 500 nm

formed at room temperature was due to low packing density due to amorphous nature, whereas those films formed at higher substrate temperatures the increase in the refractive index was due to improvement in the packing density and improved stoichiometric MoO_3. Mohamed et al. [36] observed that the refractive index of the MoO_3 films decreased with the increase annealing temperature. From the above results, it revealed that the nanostructured MoO_3 films grown at 523 K were of better surface morphology and roughness in the order of 56 nm and high optical band gap which is chemically stable and electrical resistivity of $5 \times 10^4\ \Omega$ cm. Because of these properties, MoO_3 films can be used to sense different gases like ammonia, carbon monoxide and methane.

4 Conclusions

Thin films of MoO_3 were deposited on Si and glass substrates by DC reactive magnetron sputtering at different substrate temperatures. The influence of substrate temperature on the structure, surface morphology and mechanical properties of the films was investigated. The MoO_3 films deposited at 523 K were stoichiometric in nature with crystallite size 140 nm and roughness of about 33.2 nm. The microhardeness of MoO_3 films formed at 523 K was 1.1 GPa and electrical resistivity of $3.5 \times 10^4\ \Omega$ cm with refractive index of 2.10. It is concluded that the MoO_3 films deposited at substrate temperature of 523 K can be used to sense the different gases. Sensitivity of the MoO_3 films is appreciable towards different gases due to the formation of sub oxides of molybdenum.

References

1. C. Liu, Z. Li, Z. Zhang, Electrochimca Acta **134**, 84 (2014)
2. M.J. Lee, S.I. Kim, B. Lee, H. Yin, S.E. Ahn, B.S. Kang, K.H. Kim, J. Park, C.J. Park, I. Song, S.W. Kim, G. Stefanovich, J.H. Lee, S.J. Hung, Y.H. Kim, Y. Park, Adv. Funct. Mater. **19**, 1587 (2009)
3. Y.X. Li, Q.B. Yang, X.F. Yu, A. Trinchi, Adv. Mater. **24**, 5408 (2012)
4. A. Arfaoui, S. Touihri, A. Mhamdi, A. Labidi, T. Manoubi, Appl. Surf. Sci. **357**, 1089 (2015)
5. R. Pandeeswari, B.G. Jayapraksah, Biosens. Bioelectron. **53**, 182 (2014)
6. Y. Sen, Y. Yang, F. Hu, Y. Xiao, P. Yan, Z. Li, Mater. Sci. Semicond. Process. **29**, 250 (2015)
7. K.A. Gesheva, T. Ivanova, F. Hamelmann, J. Opt. Elect. Adv. Mater. **7**, 1243 (2005)
8. M. Rouhani, J. Hobley, G.S. Subramanian, I.Y. Phang, Y.L. Foo, S. Gorelik, Sol. Energy Mater. Sol. Cells **126**, 26 (2014)
9. J. Baltrusaitis, B.M. Sanchez, V. Fernandez, R. Veenstra, N. Dukstiene, A. Roberts, N. Failey, Appl. Surf. Sci. **326**, 151 (2015)
10. G.G. Allogho, P.V. Ashrit, Thin Solid Films **520**, 2326 (2012)
11. M.F. Al-Kuhaili, S.M.A. Durrani, I.A. Bakhtiari, A.M. Al-Shukri, Opt. Commun. **283**, 2857 (2010)
12. M.C. Rao, K. Ravindranadh, A. Kasturi, M.S. Shekhawat, Res. J. Recent Sci. **2**, 67 (2013)
13. M. Vasilopoulou, I. Kostis, A.B. Douvas, D.G. Georgiadou, A. Soultati, G. Papadimitropoulos, N.A. Stathopoulos, S.S. Savaidis, P. Angitis, D. Davazoglou, Surf. Coat. Technol. **230**, 202 (2013)
14. M. Dhanasankar, K.K. Purushothaman, G. Muralidharan, Appl. Surf. Sci. **257**, 2074 (2011)
15. H.M. Martinez, J. Torres, L.D.L. Gorreno, M.E.R. Garcia, Mater. Character **25**, 184 (2013)
16. B.M. Sanchez, T. Brousse, R. Castro, V. Nicolos, P.S. Grant, Electrochem. Acta **91**, 253 (2013)
17. V.K. Sabhapathi, O.M. Hussian, S. Uthanna, B.S. Naidu, P.J. Reddy, M. Julien, M. Balkanski, Mater. Sci. Eng. B **32**, 93 (1995)
18. W.Q. Yang, Z.R. Wei, X.H. Zhu, D.Y. Yang, Phys. Lett. A **373**, 3965 (2009)
19. K. Srinivasa Rao, B. Rajini Kanth, P.K. Mukhopadhyay, Appl. Phys. A **96**, 985 (2009)
20. C.V. Ramana, V.V. Atuchin, V.G. Kesler, V.A. Kochubey, L.D. Pokrovsky, V. Shutthanadan, U. Becker, R.C. Ewing, Appl. Surf. Sci. **253**, 5368 (2007)
21. M.S. Oh, B.S. Yang, J.H. Lee, S.H. Oh, U.S. Lee, Y.J. Kim, H.J. Kim, M.S. Huh, J. Vac. Sci. Technol. A **30**, 031501 (2012)
22. P.S. Wang, J.W. Wu, W.H. Tseng, M.H. Chen, C.I. Wu, Appl. Phys. Lett. **98**, 173302 (2011)
23. X. Fan, G. Fang, P. Qin, N. Sun, N. Liu, Q. Zheng, L. Yuan, X. Zhao, J. Phys. D Appl. Phys. **44**, 045101 (2011)
24. W.C. Chang, X. Qi, J. Kuo, S. Lee, S. Ng, D. Chen, Cryst. Eng. Commun. **13**, 5125 (2011)
25. V. Nirupama, K.R. Gunasekhar, B. Sreedhar, S. Uthanna, Curr. Appl. Phys. **10**, 272 (2010)
26. S. Uthanna, V. Nirupama, J.F. Pierson, Appl. Surf. Sci. **256**, 3133 (2010)
27. V. Nirupama, B. Sreedhar, S. Uthanna, J. Mater. Sci. Mater. Electron. **21**, 45 (2010)
28. V. Nirupama, S. Uthanna, J. Optoelectron. Adv. Mater. **11**, 320 (2009)
29. S. Nathan, G.K. Muralidhar, G. Mohan Rao, Vacuum **49**, 3304 (1998)
30. A. Quintana, A. Varea, M. Guerrero, S. Surinach, M.D. Baro, J. Sort, E. Pellicer, Electrochem. Acta **173**, 705 (2015)
31. B.E. Warren, *X-ray Diffraction* (Dover, New York, 1990), p. 253
32. Y.P.V. Subbaiah, P. Prathap, M. Devika, K.T. Ramakrishna Reddy, Phys. B **365**, 240 (2005)
33. S.S. Sunu, E. Prabhu, V. Jayaraman, K.I. Gnanasekhar, T. Gnanasekharan, Sens. Actuators B **94**, 189 (2003)
34. R. Sivakumar, V. Vijayan, V. Ganesan, M. Jayachandran, C. Sanjeeviraja, Smart Mater. Struct. **14**, 204 (2005)
35. T. Tsai, K. Maruya, M. Ai, A. Ozaki, Bull. Chem. Soc. Jpn. **55**, 949 (1982)
36. S.H. Mohammed, S. Venkataraj, Vacuum **81**, 636 (2007)
37. G.E.B. Core, G. Abello, A.H. Klahn, A. Lucero, M.V. Nunez, B. Torrejon, C. Castillo, Polyhedron **29**, 1551 (2010)
38. G. Alcala, P. Skeldon, G.E. Thompson, A.B. Mann, H. Habazaki, K. Shimizu, Nanotechnology **13**, 451 (2002)
39. D. Rafaja, H. Kostenbauer, U. Muhle, C. Loffler, G. Shreber, M. Kathrein, J. Winkler, Thin Solid Films **528**, 42 (2013)
40. A.E. Hady, B. Kashyout, H.M.A. Soiman, H.A. Gabal, P.A. Ibrahim, M. Fathy, Alex. Eng. J. **50**, 57 (2011)
41. N.F. Mott, E.A. Davis, *Electroni Processes in Non-crystalline Materials* (Clarendon, Oxford, 1971), p. 213
42. S. Krishna Kumar, C.S. Menon, Bull. Mater. Sci. India **16**, 187 (1993)